Biochemical and Biophysical Research Communications 441 (2013) 25–30

Contents lists available at ScienceDirect

Biochemical and Biophysical Research Communications

journal homepage: www.elsevier.com/locate/ybbrc

Possible involvement of Hcn1 ion channel in learning and memory dysfunction in SAMP8 mice

Maruf Mohammad Akbor [a], Koji Tomobe [b,3], Tomomi Yamada [a], Juhyon Kim [c], Hiroki Mano [a,1], Nobuyuki Kurosawa [a], Kazuo Sasaki [c], Yasuyuki Nomura [b,2], Masaharu Isobe [a,*]

[a] Laboratory of Molecular and Cellular Biology, Faculty of Science and Engineering, Graduate School, University of Toyama, 3190 Gofuku, Toyama-shi, Toyama 930-8555, Japan
[b] Department of Pharmacology, Graduate School of Pharmaceutical Sciences, Hokkaido University, Sapporo 060-0812, Japan
[c] Division of Bio-Information Engineering, Faculty of Engineering, University of Toyama, 3190 Gofuku, Toyama 930-8555, Japan

ARTICLE INFO

Article history:
Received 19 September 2013
Available online 11 October 2013

Keywords:
SAMP8
Chromosome 13
QTL analysis
RNA-seq analysis
Learning and memory deficiency
*Hcn*1

ABSTRACT

The senescence-accelerated mouse prone 8 (SAMP8) strain exhibits age-related learning and memory deficits (LMD) at 2 months of age. Combined linkage analysis of 264 F2 intercross SAMP8 × JF1 mice and RNA-seq analysis identified *Hcn*1 gene out of 29 genes in the LMD region on chromosome 13. *Hcn*1 in SAMP8 strain showed 15 times less polyglutamine repetition compared to Japanese fancy mouse 1 (JF1). Whole cell patch clamp analysis showed that Hcn1 ion conductivity was significantly lower in SAMP8 compared to that of JF1, which may be associated with learning and memory deficiency.

1. Introduction

In every advanced nation where life expectancy increases, the incidence of age-related dementia increases simultaneously. The exact cause of age-related dementia is still unknown due to involvement of multifactorial genes.

The senescence-accelerated mouse prone 8 (SAMP8) strain exhibits severe age-related learning and memory deficits (LMD) at 2 months of age well before the median age of survival (17.2 months), which further aggravates with advancing age without displaying other signs of premature aging [1]. Japanese Fancy Mouse (JF1) strain shows normal learning and memory [2]. In a previous study, we have performed genetic analysis of SAMP8 mouse using the whole genome scan for quantitative trait loci (QTLs) to specify the impairment in step-through passive avoidance response with F2 intercross SAMP8 × JF1 mice and 5 loci have been identified with significant linkage to chromosomes 1, 12, 13 and 15 related to manifestations of LMD [3]. To narrow down the candidate regions and to assess candidate genes, we performed linkage analysis with additional markers on chromosome 13 and placed the LMD locus between D13Mit53 and D13Mit78 marker. By combining linkage analysis and RNA-seq analysis, Hyperpolarization activated cyclic nucleotide gated potassium channel 1 (*Hcn*1) gene was strategically identified out of 29 genes in the LMD region.

Hcn1 encodes K^+ ion permeable channel consists of six α-helical segments (S1–S6). There is a CAG repetition known as polyglutamine (polyQ) repetition region at the C-terminal end of this channel. The current flowing through Hcn channel plays a key role in the control of cardiac and neuronal rhythmicity. The current carried by Hcn channels is important for generating and pacing rhythmic bursts in many brain areas, including the septum. Recent studies suggest roles for Hcn channels in coordinated motor behavior and aspects of learning and memory [4,5].

Interestingly, we found that the PolyQ repetition in the C-terminal end of Hcn1 is 15 times less in case of SAMP8 (22 CAG repeats) compared to JF1 (37 CAG repeats). Whole cell patch clamp analysis of 293FT cells transiently expressed *Hcn*1 genes revealed that ion conductivity of SAMP8-type Hcn1 was significantly lower than that of the JF1 mice. Present results demonstrated possibility that the Hcn1 channel mutation causes learning and memory dysfunction in SAMP8 strain.

* Corresponding author. Fax: +81 76 445 6874.
E-mail address: isobe@eng.u-toyama.ac.jp (M. Isobe).
[1] Current address: Department of Molecular Neuroscience, Graduate School of Medicine and Pharmaceutical Sciences, University of Toyama, Toyama, Japan.
[2] Current address: Department of Pharmacology, Kurume University School of Medicine, 67 Asahimachi, Kurume 830-0011, Japan
[3] Current address: Department of Pathophysiology, Yokohama College of Pharmacy, Matano-cho 601, Totsuka-ku, Yokohama 245-0066, Japan.

0006-291X/$ - see front matter © 2013 Elsevier Inc. All rights reserved.
http://dx.doi.org/10.1016/j.bbrc.2013.09.145

2. Materials and methods

2.1. QTL analysis

Animal experiments have been approved and conducted according to the guidelines of ethical review committee by Hokkaido University. QTL analysis was performed as described previously [3]. Briefly, genomic DNA was extracted from mice tail by standard procedures. Microsatellite sequence length polymorphisms were detected by 2% agarose gel electrophoresis after polymerase chain reaction. A genetic mapping study of F2 intercross SAMP8 × JF1 mice was performed through passive avoidance test, in which SAMP8 exhibiting short retention time and JF1 exhibiting normal long retention time. Linkage analysis was performed with interval mapping by Mapmaker/QTL 3.0 b 29 software [www.mapmanager.org]. 155 informative markers were used to perform individual genotyping of 264 F2 mice (145 females and 119 males). The position of microsatellite markers are followed according to the UCSC Genome Bioinformatics (http://genome.ucsc.edu/cgi-bin/hgGateway).

2.2. RNA-seq and micro array analysis

Hippocampus mRNAs obtained from 2 months of age mice were extracted with trizole method as described previously [6]. RNA-seq analysis was performed using hippocampus mRNA of 2 months of age mice by Hokkaido System Science (http://www.hssnet.co.jp/index_e.htm). RNA-seq data were analyzed for SAMP8 specific polymorphism such as single nucleotide polymorphism (SNPs), triad base repetition, unique alternative splicing events and long intervening non coding RNAs by using Integrated Genomic viewer version 2.0 (IGV 2.0) [7].

Micro array analysis was performed using Agilent sure print G3 mouse gene expression 8X60K array using total RNAs of 2 and 5 months of age both male and female mice of JF1 and SAMP8 strain through Takara bio (http://www.clontech.com/takara).

2.3. CAG repeat analysis

The CAG repeat region located in the *Hcn*1 gene in JF1 and SAMP8 was amplified by PCR with primers 5′-CTCAGCAGCAACTACCGCAGTC-3′ and 5′-GGAGACCTCATGGGGCAGAGAAGGC-3′. Approximately 10 ng genomic DNA was amplified with PrimeStar DNA polymerase with My Cycler™ Thermal Cycler, BIO RAD (One cycle with denaturation at 96 °C for 2 min followed by 30 cycles with denaturation at 96 °C for 10 s, annealing at 55 °C for 10 s and strand extension at 72 °C for 1 min, followed by a final extension of 5 min at 72 °C). PCR products were sub cloned into pBlue Script SK (−) and sequenced with ABI 377 DNA Sequencer (Applied Biosystems).

2.4. Construction of expression vectors

Full length of *Hcn*1 gene of SAMP8-type and JF1-type were amplified by RT-PCR using hippocampus cDNA as templates with primers 5′-TGCTCCTTGGCTTCGAGCCCCCGGCGAGATC-3′ and 5′-TCTTTTGAACTTCTCTTGGGCATTTAGATA-3′. The amplified genes were inserted into pGEM-T-easy vector and sequenced. The SAMP8 type- and JF1 type-*Hcn*1 gene were then inserted into pEGFP-C1 (Clontech), respectively. P2A sequence encoding GSGATNFSLLKQAGDVEENPGP was synthesized by annealing oligonucleotides and then inserted in frame between green fluorescent protein (GFP) and *Hcn*1 gene to construct pEGFP-P2A-HCN1 (SAMP8) and pEGFP-P2A-HCN1 (JF1) respectively. SAMP8 type- and JF1 type-*Hcn*1 gene were also inserted into pIRES2-EGFP, resulting in the generation of pIRES-HCN1 (SAMP8) and pIRES-HCN1 (JF1) respectively. Plasmids were prepared by high purity midiprep plasmid purification kit (Marligen Bioscience) and suspended in ultrapure water.

2.5. Transient expression of Hcn1 in 293FT cells

293FT cells were cultured in 3 cm culture dish with 2 ml DMEM containing 10% fetal bovine serum under 5% CO_2 incubator. Plasmid DNA was transfected with FuGENE HD Transfection Reagent (Roche Co.) as described previously [8].

2.6. Western blotting method

Cells were harvested after 48 h of the DNA transfection and lysed with 500 μl RIPA buffer containing 5 μl of protease inhibitor (Sigma–Aldrich), 2.5 μl of 200 mM NaF, 1 μl of 500 mM Na_3VO_4, 5 μl of 0.1 M DTT. Supernatant was collected by centrifugation 15 × 1000 rpm for 10 min at 4 °C, then run in 10% SDS–polyacrylamide gel. Proteins were transferred to PVDF filter from gel. Hcn1 and GFP were detected with anti-Hcn1 (CHEMICON Co.) and anti-GFP antibody (Roche Co.). Signals were revealed by using a Chemi-Lumi One (Nakarai tesque, Japan) as described previously [6]. Images were captured using CCD camera (Fujifilm, Lumino Image Analyzer, LAS-1000-mini, Japan). The intensity of Hcn1 and EGFP brands were quantified using image analysis software Image J (ver. 1.46r) (http://imagej.nih.gov/ij/index.html).

2.7. Immunostaining method

Cells expressing Hcn1 were fixed with PBS containing 4% formalin for 10 min, washed three times with 1× PBS containing 0.5% Triton X-100. Hcn1 was detected with anti-Hcn1 antibody (CHEMICON Co.) combined with Anti-Rabbit IgG Antibody labeled with Alexa594 (Invitrogen Co.). Signals were observed by fluorescence microscopy (1X71S1F-2, Olympus, Tokyo, Japan) and images were captured using CCD camera (KEYENCE-VB7010, Japan).

2.8. GFP-based cell marking for whole cell patch clamp recording

8×10^5 293FT cells plated on collagen coated 3 cm culture were transiently transfected with plasmid. After 48 h of the transfection, culture dish was put as a whole cell patch clamp recording chamber on the stage of an upright microscope (BX-50WI, Olympus, Tokyo, Japan). Then, extracellular solution containing 30 mM KCl, 110 mM NaCl, 0.5 mM $MgCl_2$, 1.8 mM $CaCl_2$, 5 mM HEPES, pH was adjusted to 7.3 and replaced nutrient medium in the culture dish, and was perfused at 1 ml/min and at room temperature. GFP-labeled cells were visualized on a television screen through an infrared charge coupled device (CCD) camera (C2741-79, Hamamatsu Photonics, Hamamatsu, Japan) and a real-time digital video microscopy processor (XL-20, Olympus, Tokyo, Japan). Cells exhibiting similar intensity level of GFP fluorescence were chosen for the whole cell patch clamp study. Whole cell patch clamp recordings were made on the cell. Patch pipettes were pulled from 1.5 mm o.d. borosilicate glass (1.5 × 90 mm, GD 1.5, Narishige, Japan) and had resistances of 3–6 MΩ when filled with the standard pipette solution containing 130 mM KCl, 10 mM NaCl, 0.5 mM $MgCl_2$, 5 HEPES, 1 EGTA, pH adjusted to 7.3. Cells were recorded in voltage clamp mode with holding potential of −40 mV using a patch clamp amplifier (Axopatch 200B, Axon Instruments, Union City, CA, USA). To activate Hcn channels, the cells were applied voltage step pulses (from −140 to −10 mV) with pulse duration of 3 s and inter pulse intervals of 2 s. An Ag/AgCl reference electrode was placed near the intermediate position between the inlet and outlet of the chamber.

Currents recorded via the electrodes were fed into the amplifier. The output of the amplifier was digitized using an A/D converter board (Digidata 1200, Axon Instruments, Union City, USA) with a sampling rate of 10 kHz, and recorded on a hard disk by data acquisition and analysis software (pCLAMP 8, Axon Instruments, Union City, USA). Membrane potentials were low-pass filtered at 2 kHz.

2.9. Statistical analysis

All data were expressed as means ± SEMs. The statistical significance between genotype and phenotype was analyzed using JMP® ver. 10.0.2 (http://www.jmp.com) followed by Turkey and Kramer's honestly significance difference test. For comparison of multiple gene groups, two-way analysis of variance (ANOVA) with repeated measures followed by a Scheffe's F test was used. $P < 0.05$ was taken as the level of statistical significance.

3. Results

3.1. Identification of candidate gene by QTL analysis of chromosome 13

To clarify the fundamental determinants involved in age-related LMD in SAMP8 strain, linkage analysis was performed with additional markers. Genotyping data is significant ($P < 0.01$) only when female mice was considered in case of P8/P8 vs. JF1/JF1 and JF1/JF1 vs. P8/JF1 (Table 1). As shown in Fig. 1A, high logarithm of the likelihood ratio for linkage (lod) score peak was obtained in F2 intercross SAMP8 × JF1 female mice of chromosome 13 and marked as LMD region. The LMD region, showing high lod score value 2.2–3.2 was placed between D13Mit53 marker and D13Mit78 marker. The position of highest lod score value 3.2 was observed at D13Mit77 marker in LMD region.

There were 29 genes between D13Mit53 marker and D13Mit78 marker. To identify candidate genes underlying QTLs, we performed RNA-seq and micro array analysis. Micro array analysis of these genes showed no significant differences in the level of gene expression between SAMP8 and JF1 strains (Supplementary Table S1). Interestingly, RNA-seq data analysis identified *Hcn*1 gene with differences in CAG (Glutamine, Q) repetition length in SAMP8 mice compared to JF1 mice (Fig. 1B).

To evaluate the differences in CAG repeat between SAMP8 and JF1, PCR amplification of genomic DNA using primers flanking the CAG repeat region in the *Hcn*1 gene was performed and subsequently electrophoresed. The size of SAMP8 band (185 bp) is smaller than JF1 band (230 bp) (Fig. 1C). Nucleotide sequencing of the PCR products demonstrated that 15 CAG triad base pairs were missing in SAMP8 mice (22 CAG repeats) compared to JF1 mice (37 CAG repeats) while normal wild type mice (C57BL/6, BALB/C strains) possessed 38 CAG repeats (Fig. 1D).

3.2. Stoichiometric production of EGFP and Hcn1 proteins in cells by P2A-based bicistronic plasmid

In transient transfection system, gene expression levels are controlled by the amount of plasmid used for the transfection and the expression levels are highly heterologous. Because trans-membrane current depends on the number of channel expressed on a cell, a uniform expression level of the channel protein per cells is desirable to perform the whole cell patch clamp analysis. To monitor accurately the amount of Hcn1 ion channel expression per cell, we constructed P2A-based bicistronic plasmids, which allow the stoichiometric production of both upstream and downstream protein [9–11]. The complete cleavage at P2A sites that produce GFP-P2A fusion protein and Hcn1 was determined by Western blotting (Fig. 2A). Immunofluorescent analysis of 293FT cells transiently transfected with GFP-P2A-HCN1 expression plasmids revealed that all cells expressing GFP were positive for Hcn1 (Fig. 2B). When we measured the florescent intensity of GFP in relation to that of Hcn1, high R-value of linear regression line was obtained in cells transiently transfected with pEGFP-P2A-HCN1 (SAMP8) and pEGFP-P2A-HCN1 (JF1), respectively ($R^2 = 0.93$ for SAMP8 and 0.85 for JF1) (Fig. 2C). However, low R-value for the correlation between GFP and Hcn1 was obtained in cells transiently transfected with pIRES-HCN1 (SAMP8) and pIRES-HCN1 (JF1), ($R^2 = 0.37$ for SAMP8 and 0.64 for JF1) (Supplementary Fig. S2). So by measuring the fluorescence of GFP on cells transiently transfected with EGFP-P2A-HCN1 constructs, we can more precisely monitor the level of Hcn1 expression in each cell by the P2A than the IRES constructs.

3.3. Hcn1 channels of SAMP8 strain showed decreased current value by patch-clamp analysis

Cells with similar florescent intensity of GFP (JF1: 634 ± 7, SAMP8: 852 ± 9) were selected and used for patch clamp recording. To activate Hcn1 channels, the recorded cells were applied voltage step pulses. The leak currents were digitally subtracted. In total, 57 cells were recorded. As shown in Fig. 3A, the GFP cell did not show inward currents (left panel), suggesting 293FT cells have few intrinsic Hcn channels. The voltage step pulses elicited inward currents on cells expressing SAMP8-type Hcn1, however the amplitudes of currents were less than those obtained in JF1 transfectant (Fig. 3B).

Post hoc analysis revealed that both the JF1 and the SAMP8 groups showed significantly greater amplitudes of voltage-dependent currents than the GFP group ($P < 0.01$ for each), however that of the SAMP8 group was significantly lower than that of the JF1 group ($P < 0.05$). When each current value was normalized by fluorescence intensity of each cell, significant difference of amplitude of the currents was also detected between JF1 and the SAMP8 groups ($P < 0.01$), denying the possibility that the difference of

Table 1
Results of ANOVA for LMD at 5 months.

Gender	Retention time by marker genotype			$P1$-value†	$P2$-value††	$P3$-value†††
	P8/P8	P8/JF1	JF1/JF1			
Male	219.6 ± 39.3 (28)	242.6 ± 32.4 (62)	328.9 ± 41.7 (29)	0.9055	0.1960	0.2431
Female	173.0 ± 23.6 (32)	226.5 ± 24.7 (79)	382.9 ± 55.5 (34)	0.5061	0.0028*	0.0117*
Male + female	194.8 ± 22.3 (60)	233.5 ± 19.8 (141)	358.0 ± 35.5 (63)	0.5326	0.0004*	0.0016*

D13 Mit77 marker was used for genotyping of chromosome 13 LMD locus. All the data are expressed as mean ± S.E.M. No. of mice is indicated in parentheses.
† $P1$-value indicating genotyping data of P8/P8 vs. P8/JF1.
†† $P2$-value indicating genotyping data of P8/P8 vs. JF1/JF1.
††† $P3$-value indicating genotyping data of JF1/JF1 vs. P8/JF1.
* Dominances are determined only when P value is less than 0.05.

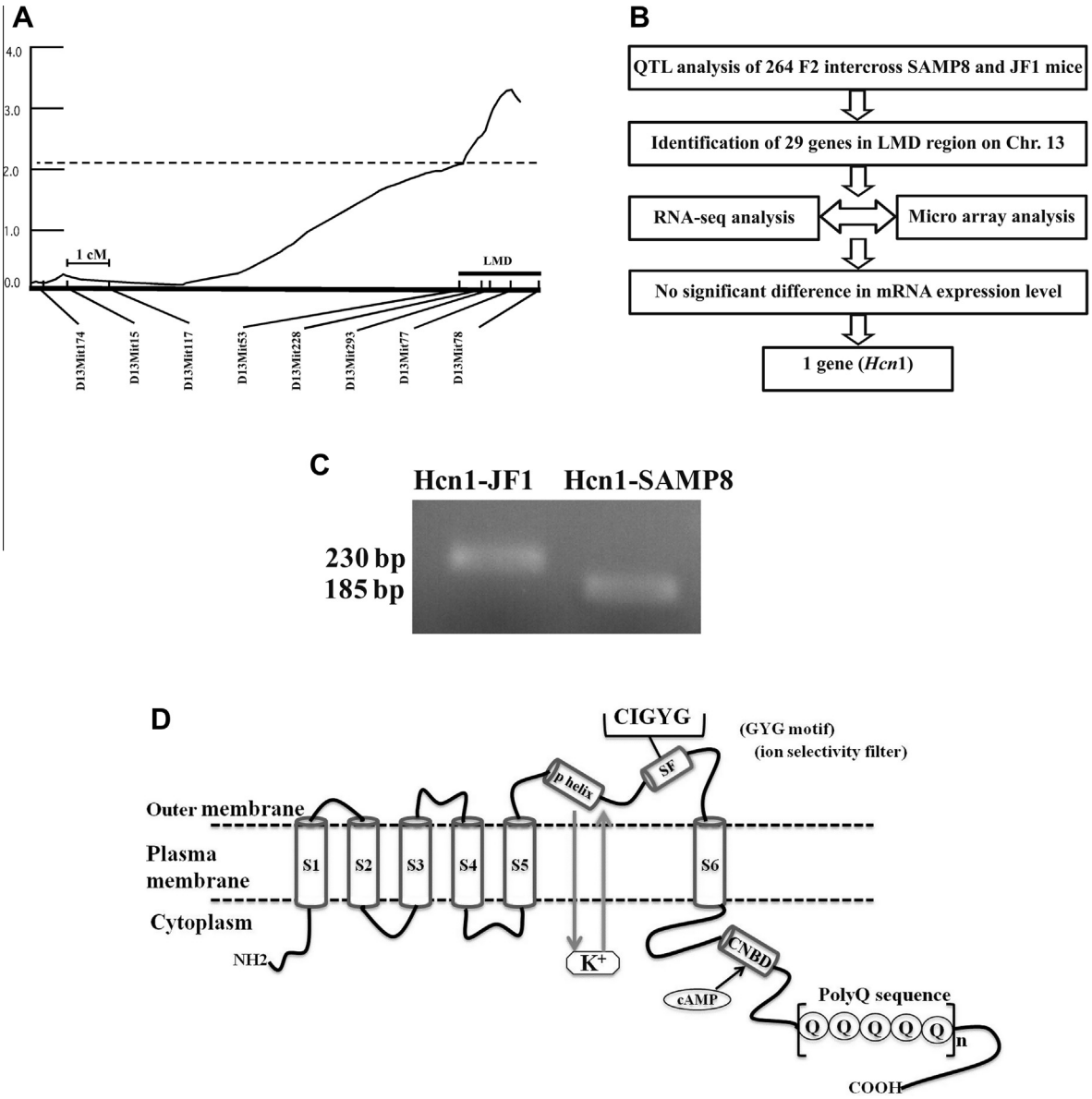

Fig. 1. *Hcn*1 is the candidate LMD gene on chromosome 13. (A) Lod score plots for LMD strain on chromosomes 13. *X*-axis: indicates map position in centi-Morgan (cM). Microsatellite markers are indicated. *Y*-axis: lod scores for QTL in (SAMP8 × JF1) F2 progeny. Female scores were standardized and analyzed by Mapmaker/QTL. Dotted horizontal line on lod score plot indicates the lod = 2.2 as limits for suggestive level. Thick small horizontal line indicates the 1-lod support interval for the noted LMD locus. (B) Flow chart summarizing the strategy for identification of candidate gene on mouse chromosome 13. (C) Agarose gel of PCR fragments obtained along the CAG repeated region of the *Hcn*1 gene. (D) Schematic diagram of Hcn1 channel structure. The six putative transmembrane segments (S1–S6) and the position of polyQ repeat are shown. Here, *n* represents number of CAG repetitions = 22 for SAMP8 and 37 for JF1.

the GFP fluorescence intensity might cause differences of current amplitude (Supplemental Fig. S3).

These results indicate that amount of trans-membrane currents via the Hcn1 channels of SAMP8 mice is smaller than that of JF1 mice.

4. Discussion

By combined linkage and RNA-seq analysis, we identified *Hcn*1 has structural differences in the length of CAG repeats between SAMP8 and JF1 strains, resulting less ion conductivity in cells expressing SAMP8-type Hcn1 compared to those of JF1.

Hcn1 ion channel has been found in correlation with learning and memory function in many studies [12,13]. Activation of the Hcn channels, known as "pacemaker channels", causes hyperpolarization-activated depolarization, which contributes to modulation of neuronal spike timing. In central nerves system, spike timing is recognized as an important factor to elicit synaptic plasticity, which may relate to learning and memory. Recent reports demonstrated that inhibition of Hcn channel by ZD7288 blocker can block the induction of long term potentiation (LTP) [14]. Septal Hcn channels likely influence memory by contributing to the theta rhythm and thus influencing memory processing in the hippocampus. Cissé et al. demonstrated that septal infusions of the Hcn channel blocker ZD7288 impair hippocampal theta, an effect that would be expected to impair memory [5]. These reports are consistent with our findings that the reduced ion conductivity of SAMP8-type Hcn1 in relation with LMD. On the contrary, Hussaini et al. found that knockdown of Hcn1 ion channels in mice facilitate spatial learning and memory [15]. In Hcn1 knockout mice alternative neuronal circuit formation during brain development may compensate Hcn1 channel ion conductivity deficiency [16].

A growing number of neurodegenerative diseases have been found resulting from the expansion mutation of an unstable polyQ

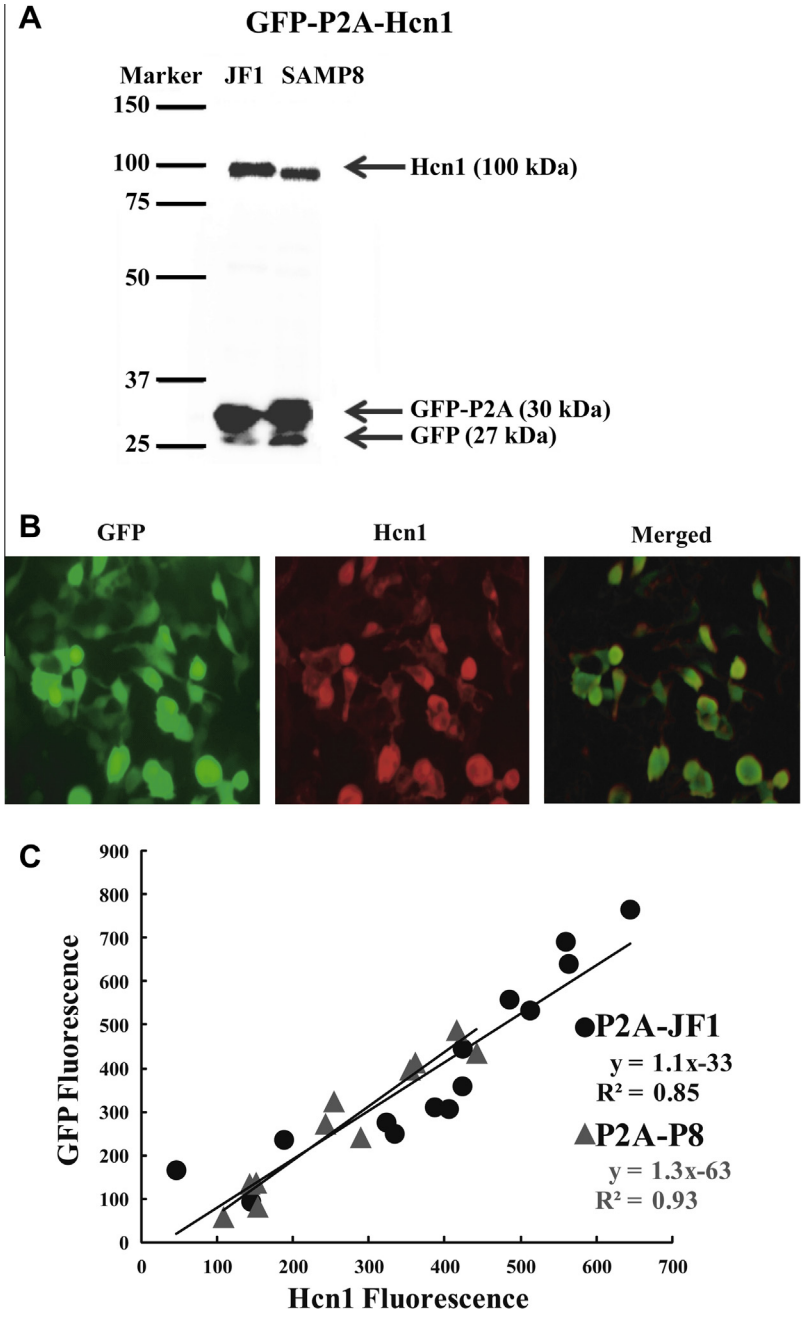

Fig. 2. P2A enables coordinate expression of GFP and Hcn1. (A) WB analysis of cleavage efficiency of the P2As in 293FT cells. The cleavage efficiency was assessed using GFP and Hcn1 antibodies, respectively. (B) Immunofluorescent images of 293FT cells transiently transfected with GFP-P2A-HCN1 (SAMP8) construct representative images are shown. (C) Linear regression analysis of measured fluorescent intensity of GFP values in relation to that of Hcn1. Fluorescent intensity for GFP and Hcn1 expressed in each cell was measured by ImageJ software and expressed as arbitrary unit. R^2-values of linear regression line were shown.

[17–19]. Protein aggregation, which is a key feature of most of these diseases, is thought to be triggered by these expanded polyQ sequences in disease-related proteins. In human, the length of CAG repeats of *HCN*1 gene is shorter and interrupted by other sequences. Therefore, the expansion of CAG repeats in human *HCN*1 gene less likely to occur. It has been shown that polyQ tracts in proteins stabilize protein interaction and regulate various signaling processes [20,21]. Alteration of this important biological function due to polyQ reduction may unstabilize protein interactions, leading to less ion conductivity as we observed in SAMP8 strain.

There are several methods to monitor foreign genes expression including co-transfection, fusion protein and bicistronic expression. In cotransfection, not all cells can express cotransfected genes. Due to high molecular weight of EGFP, possible impact of EGFP fusion was also considered. IRES allows coordinate expression of two or more genes from a single transcript. Thus, detection of the GFP fluorescence encoded by the second cistron is evidence that the first cistron is also being expressed. However expression of the downstream gene was found to be as much as 10-fold lower than the upstream gene [22–24]. Furthermore we found that IRES failed to express Hcn1 and GFP in a coordinate manner (Supplemental Fig. S2). By using P2A sequence, we were able to monitor Hcn1 ion channel expression that allowed us more precisely to estimate Hcn1 expression in cell to conduct whole-cell patch clamp analysis.

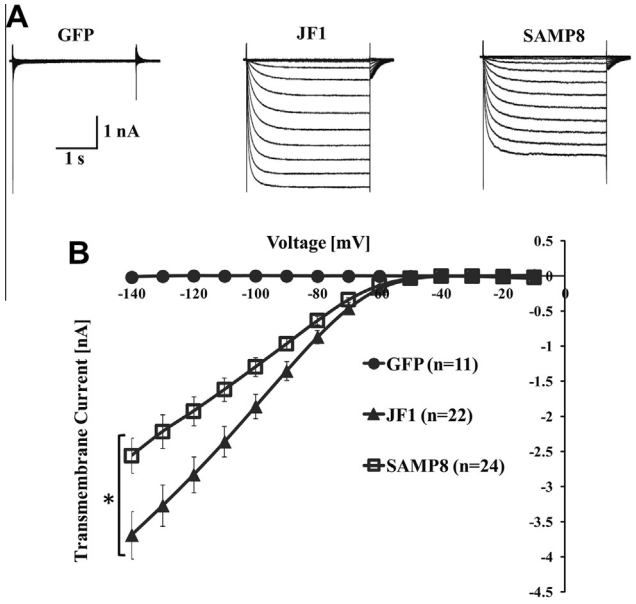

Fig. 3. Difference in polyQ repetition affects ion permeability of Hcn1. (A) Comparison of membrane currents among GFP-, GFP-P2A-JF1, and GFP-P2A-SAMP8 expressing cells. Transmembrane current in response to a series of square pulses of 3 s duration measured using the voltage clamp setup. The transmembrane potential in these experiments ranged from −10 to −140 mV in steps of −10 mV. Data are shown for representative cells. (B) Current–voltage relationships. *Amplitude of voltage-dependent currents of the SAMP8 group was lower than that of JF1 group ($P < 0.05$).

In Senescence-resistant inbred strain 1 (SAMR1) showed normal aging with non-thymic lymphoma, histiocytic sarcoma and ovarian cysts [1], normally used as aging control strain for the SAMP8. Although SAMR1 strain has the same length of CAG repetition like SAMP8, they did not show any severe learning and memory dysfunction. Considering SAMP8 has 5 LMD loci, *Hcn1* is not enough to cause learning and memory dysfunction alone thoroughly in SAMR1 strain. Combination with genes from other loci may affect learning and memory deficiency in SAMP8 mice, although further studies are required. Gender difference in mice may also have influence on the phenotypic behavior. We found SAMP8 male did not show significance in LMD marker genotype. Flood et al. demonstrated that decreased level of plasma testosterone in SAMP8 mice contribute to the age-related deficit in learning and memory, while replacement improves age-related impairment of learning and memory function which clearly supports our study [25].

In conclusion, *Hcn*1 is the only the most promising candidate gene on chromosome 13 may be correlated with learning and memory dysfunction in SAMP8 mice strain.

Acknowledgments

This work was supported in part by funds from the Ministry of Education, Culture, Sports, Science and Technology (MEXT)-Japan and the Hokuriku Life Science Cluster of Regional Innovation Strategy Support Program.

We thank the members of our laboratory including Yasuyuki Teranaka, Woong Kim and Ai Sato for technical assistance and fruitful discussions.

Appendix A. Supplementary data

Supplementary data associated with this article can be found, in the online version, at http://dx.doi.org/10.1016/j.bbrc.2013.09.145.

References

[1] T. Takeda, M. Hosokawa, K. Higuchi, Senescence accelerated mouse (SAM): a novel murine model of accelerated senescence, J. Am. Geriatr. Soc. 39 (1991) 911–919.
[2] T. Koide, K. Moriwaki, K. Uchida, A. Mita, T. Sagai, H. Yonekawa, H. Katoh, N. Miyashita, K. Tsuchiya, T.J. Nielsen, T. Shiroishi, A new inbred strain JF1 established from Japanese fancy mouse carrying the classic piebald allele, Mamm. Genome 9 (1998) 15–19.
[3] M. Isobe, K. Tomobe, M. Sawada, A. Kondo, N. Kurosawa, Y. Nomura, Quantitative trait loci for age-related memory dysfunction in SAMP8 and JF1 mice, Int. Congr. Ser. 1260 (2004) 29–34.
[4] C. Wahl-Schott, M. Biel, HCN channels: structure, cellular regulation and physiological function, Cell. Mol. Life Sci. 66 (2009) 470–494.
[5] R.S. Cissé, D.L. Krebs-Kraft, M.B. Parent, Septal infusions of the hyperpolarization-activated cyclic nucleotide-gated channel (HCN-channel) blocker ZD7288 impair spontaneous alternation but not inhibitory avoidance, Behav. Neurosci. 122 (3) (2008) 549–556.
[6] N. Kurosawa, R. Fujimoto, T. Ozawa, T. Itoyama, N. Sadamori, M. Isobe, Reduced level of the BCL11B protein is associated with adult T-cell leukemia/lymphoma, PLoS One 8 (1) (2013) e55147.
[7] J.T. Robinson, H. Thorvaldsdóttir, W. Winckler, M. Guttman, E.S. Lander, G. Getz, J.P. Mesirov, Integrative genomics viewer, Nat. Biotechnol. 29 (2011) 24–26.
[8] N. Kurosawa, M. Yoshioka, R. Fujimoto, F. Yamagishi, M. Isobe, Rapid production of antigen-specific monoclonal antibodies from a variety of animals, BMC Biol. 10 (2012) 80.
[9] C. Halpin, S.E. Cooke, A. Barakate, A.E. Amrani, M.D. Ryan, Self-processing 2A-polyproteins – a system for co-ordinate expression of multiple proteins in transgenic plants, Plant J. 17 (4) (1999) 453–459.
[10] P.D. Felipe, M.R. Ryan, Targeting of proteins derived from self-processing polyproteins containing multiple signal sequences, Traffic 5 (2004) 616–626.
[11] M. Samalova, M. Fricker, I. Moore, Ratiometric fluorescence-imaging assays of plant membrane traffic using polyproteins, Traffic 7 (2006) 1701–1723.
[12] M.F. Nolan, G. Malleret, J.T. Dudman, L.B. Derek, B. Santoro, E. Gibbs, V. Svetlana, A behavioral role for dendritic integration: HCN1 channels constrain spatial memory and plasticity at inputs to distal dendrites of CA1 pyramidal neurons, Cell 119 (2004) 719–732.
[13] M.F. Nolan, G. Malleret, K.H. Lee, E. Gibbs, J.T. Dudman, B. Santoro, D. Yin, R.F. Thompson, S.A. Siegelbaum, E.R. Kandel, A. Morozov, The hyperpolarization-activated HCN1 channel is important for motor learning and neuronal integration by cerebellar purkinje cells, Cell 115 (2003) 551–564.
[14] H. Wei, Z. Cheng, G. Fu, X. Xu, Q. Lu, L. Guo, ZD7288-induced suppression of long-term potentiation was attenuated by exogenous NMDA at the schaffer collateral-CA1 synapse in the rat in vivo, Eur. J. Pharmacol. 631 (2010) 10–16.
[15] S.A. Hussaini, K.A. Kempadoo, S.J. Thuault, S.A. Seigelbaum, E.R. Kandel, Increased size and stability of CA1 and CA3 place fields in HCN1 knockout mice, Neuron 72 (2011) 643–653.
[16] X. Chen, S. Shu, L.C. Schwartz, C. Sun, J. Kapur, D.A. Bayliss, Homeostatic regulation of synaptic excitability: tonic $GABA_A$ receptor currents replace I_h in cortical pyramidal neurons of HCN1 knock-out mice, J. Neurosci. 30 (7) (2010) 2611–2622.
[17] H.Y. Zoghbi, H.T. Orr, Glutamine repeats and neurodegeneration, Annu. Rev. Neurosci. 23 (2000) 217–247.
[18] K. Nakamura, S.Y. Jeong, T. Uchihara, M. Anno, K. Nagashima, T. Nagashima, S. Ikeda, S. Tsuji, I. Kanazawa, SCA17, a novel autosomal cerebellar ataxia caused by an expanded polyglutamine in TATA-binding protein, Hum. Mol. Genet. 10 (2001) 1441–1448.
[19] K. Watase, E.J. Weeber, B. Xu, B. Antalffy, L. Yuva-Paylor, K. Hashimoto, M. Kano, R. Atkinson, Y. Sun, D.L. Armstrong, J.D. Sweatt, H.T. Orr, R. Paylor, H.Y. Zoghbi, A Long CAG repeat in the mouse Sca1 locus replicates SCA1 features and reveals the impact of protein solubility on selective neurodegeneration, Neuron 34 (2002) 905–919.
[20] S. Hands, C. Sinadinos, A. Wyttenbach, Polyglutamine gene function and dysfunction in the ageing brain, Biochim. Biophys. Acta 1779 (2008) 507–521.
[21] M.H. Schaefer, E.E. Wanker, M.A. Andrade-Navarro, Evolution and function of CAG/polyglutamine repeats in protein–protein interaction networks, Nucleic Acids Res. 40 (10) (2012) 4273–4287.
[22] M. Flasshove, W. Bardenheuer, A. Schneider, G.P. Hirsch, P. Bach, C. Bury, T. Moritz, S. Seeber, B. Opalka, Type and position of promoter elements in retroviral vectors have substantial effects on the expression level of an enhanced green fluorescent protein reporter gene, J. Cancer Res. Clin. Oncol. 126 (2000) 391–399.
[23] K. Hasegawa, A.B. Cowan, N. Nakatsuji, H. Suemori, Efficient multicistronic expression of a transgene in human embryonic stem cells, Stem Cells 25 (2007) 1707–1712.
[24] H. Mizuguchi, Z. Xu, A. Ishii-Watabe, E. Uchida, T. Hayakawa, IRES-dependent second gene expression is significantly lower than cap-dependent first gene expression in a bicistronic vector, Mol. Ther. 1 (2000) 376–382.
[25] J.F. Flood, S.A. Farr, F.E. Kaiser, M.L. Regina, J.E. Morley, Age-related decrease of plasma testosterone in SAMP8 mice: replacement improves age-related impairment of learning and memory, Physiol. Behav. 57 (4) (1995) 669–673.